https://doi.org/10.64989/rmutsbj.2026.271892

Adsorption behavior and mechanism of malachite green dye onto natural bentonite from Sa Bot district, Lopburi province, Thailand

Suchada Sawasdee* and Prachart Watcharabundit

Abstract

Dye-laden wastewater poses a persistent environmental challenge due to its toxicity and resistance to degradation. This study reports the novel application of natural bentonite sourced from Sa Bot district, Lopburi province, Thailand, for the adsorption of cationic malachite green (MG) dye. The distinct geological origin of this bentonite, which has not been previously investigated for MG dye removal, underscores its unique physicochemical properties and local relevance. Comprehensive characterization was performed using BET surface area analysis, FTIR spectroscopy, SEM-EDXS, and determination of the point of zero charge (pHpzc). Batch adsorption experiments systematically examined the effects of pH, adsorbent dose, contact time, initial dye concentration, and temperature. Optimal adsorption occurred at pH 9, with equilibrium being reached within 180 minutes, yielding a maximum adsorption capacity of 35.97mg/g at 30°C. Equilibrium data were well fitted to both Langmuir and Freundlich models, while the Redlich–Peterson model indicated surface heterogeneity. Kinetic analysis confirmed pseudo-second-order behavior, with intraparticle diffusion contributing alongside surface adsorption. Thermodynamic evaluation revealed that the process was endothermic and spontaneous across 20-40°C, as evidenced by negative ΔG values throughout this temperature range. Mechanistic insights highlighted electrostatic interactions, hydrogen bonding, n–π interactions, pore filling, and ion exchange. Furthermore, the bentonite demonstrated excellent reusability, maintaining stable performance over five regeneration cycles. These findings establish locally sourced bentonite as a cost-effective, sustainable adsorbent with practical significance for industrial wastewater treatment.

Keywords: adsorption, mechanism, malachite green dye, reusability, bentonite

Faculty of Science and Technology, Thepsatri Rajabhat University, Mueang Lopburi District, Lopburi 15000, Thailand

* Corresponding author. E-mail: suchada.s@lawasri.tru.ac.th

Received: April 30, 2026; Revised: July 17, 2026; Accepted: September 30, 2026

Introduction

The rapid expansion of industries and technological advancements have resulted in severe water pollution, with wastewater frequently containing hazardous chemicals at concentrations far exceeding WHO-recommended limits. Among these contaminants, synthetic dyes, which more than 100,000 types are currently in use, pose a major threat. As the approximately 7×10^5 to 1×10^6 tons produced annually, nearly 10-15% is discharged directly into the environment. Such wastewater originates from diverse industrial sectors, including textiles, plastics, cosmetics, and leather processing (Baidya & Kumar, 2021). Organic dyes are particularly concerning due to their vivid coloration and stable aromatic structures, which hinder natural biodegradation and allow them to persist in sewage and aquatic environments for extended periods. Their presence reduces sunlight penetration, disrupts aquatic ecosystems, and renders water unsuitable for consumption. Moreover, industrial dye emissions can contaminate food sources, thereby raising significant public health concerns (Abbas & Trari, 2020).

Malachite Green (MG) is a cost-effective and highly stable triphenylmethane-derived cationic dye extensively utilized in the textile and paper industries, as well as in aquaculture for its potent antifungal, antiprotozoal, and disinfectant properties (Abewaa et al., 2023). However, accumulating evidence demonstrates that MG is a persistent, bioaccumulate, and genotoxic compound (Li et al., 2020). Its release into aquatic environments poses serious ecological threats and is associated with carcinogenic and mutagenic effects, including gastrointestinal irritation and adverse health outcomes in humans upon ingestion (Abewaa et al., 2023; Li et al., 2020). Accordingly, the efficient removal of MG from contaminated water sources has become an urgent environmental and public health priority.

Remediation of dye-contaminated wastewater can be achieved through several primary techniques, including adsorption, chemical coagulation, biodegradation, catalyst-based reduction, cation/anion exchange, and hybrid material applications (Hakim et al., 2023). Adsorption onto solid surfaces is increasingly favored for its cost-effectiveness and ease of maintenance in large-scale operations (Ukkund et al., 2021). The interfacial interactions between the species and the adsorbent dictate adsorption phenomena. Such interactions are typically attributed to a combination of forces, such as Van der Waals forces, hydrogen bonding, hydrophobic effects, and chemical bonding (Maimulyanti et al., 2019). Although activated carbon remains a common choice due to its high adsorption performance, its practical industrial use is often hindered by high costs (Nirmaladevi et al., 2020). Consequently, there is a growing interest in utilizing sustainable inorganic materials as alternative adsorbents that offer both efficiency and economic viability.

Although these technologies offer distinct pathways for dye eradication, their real-world application must be critically evaluated based on their inherent operational trade-offs. For instance, chemical coagulation is relatively inexpensive and operationally simple, yet it demands high chemical consumption and generates a massive volume of secondary toxic sludge, which incurs substantial disposal costs (Kusumlata et al., 2024). Biodegradation represents an eco-friendly and low-cost alternative; however, the process is inherently slow, requires strict control of biological parameters, and is highly vulnerable to shock loading from toxic industrial effluents (Sehar et al., 2022). Catalytic reduction possesses a distinct advantage in terms of its eco-friendly nature. However, a

major limitation of this process is that the reaction is strictly restricted to the catalyst's surface, coupled with a heavy reliance on expensive and scarce noble metals (Ramu & Choi, 2021). Ion exchange is a technique used for the purification, separation, and decontamination of aqueous and other ion-containing solutions. However, it still possesses limitations, as it generates highly concentrated waste that requires careful disposal (Kathing & Saini, 2022). According to Dutta et al., (2021), the development of hybrid materials and nanocomposites has become a crucial approach to enhancing the efficiency of adsorption technology for dye removal. Attributed to their high specific surface area and ease of fabrication, these hybrid materials can overcome the limitations of conventional adsorbents and mitigating drawbacks associated with membrane technologies, such as their susceptibility to pore blockage.

Among the numerous advantages of clays are their low cost, wide availability, environmental compatibility, high specific surface area, superior adsorption capacity, nontoxic nature, and remarkable potential for chemical modification and ion exchange (Queiroga et al., 2019). Bentonite, in particular, is a naturally occurring, cost-effective, and eco-friendly clay that has shown considerable promise as an efficient adsorbent for dye remediation (Hamad et al., 2024). Bentonite is mainly composed of expandable montmorillonite, whose fundamental layer structure contains a single Al^{3+} octahedral sheet. Through modification processes, the clay's surface and structural properties are altered by substituting the interlayer cations (such as Na^{+}, K^{+} and Ca^{2+}) with selected species (Alexander et al., 2019). It is widely applied in environmental remediation, capturing cationic pollutants through electrostatic attraction and ion exchange driven by the negative charge of its silicate layers. Acid activation is recognized as a cost-effective method to enhance porosity and surface properties (Fernandes et al., 2020). Bentonite is widely recognized for its distinctive physicochemical properties, including a layered microporous structure, high swelling capacity, and excellent hydraulic conductivity. These intrinsic features, together with its abundant availability, enable bentonite to effectively sequester pollutants, especially cationic dyes, from aqueous solutions (Bergaoui et al., 2023; Hamad et al., 2024). Reported applications include the removal of anionic dyes (Fernandes et al., 2020), methylene blue (Momina et al., 2020), Telon Blue (Belkhodja et al., 2026), Direct Yellow 50 (Mahmoud et al., 2022), and Orange G (Taibi et al., 2023).

However, limited studies have examined raw local bentonite deposits, particularly those from Lopburi province, Thailand, under variable textile wastewater conditions. Most existing research focuses on standardized commercial clays, leaving the distinctive mineralogy and adsorption pathways of regional materials unexplored. Addressing this gap provides practical value by offering low-cost, decentralized treatment options that reduce reliance on imported adsorbents and support circular economy practices. In this study, bentonite from Lopburi province was employed as an abundant and effective adsorbent for malachite green removal through batch adsorption experiments. The effects of operational parameters (pH, dosage, contact time, initial dye concentration, and temperature) were systematically investigated to optimize performance. Adsorption isotherm models were applied to estimate maximum capacity and identify the most suitable equilibrium model, while kinetic and thermodynamic analyses elucidated the adsorption mechanism. Structural characterization (BET, FTIR, SEM-EDXS)

and reusability tests further confirmed the material's potential. These findings advance the development of cost-effective and sustainable adsorbents for dye-contaminated water treatment.

In summary, this study provides the first comprehensive mechanistic insights into the adsorption behavior of natural bentonite uniquely sourced from Sa Bot district, Lopburi province, Thailand. Its distinct physicochemical characteristics, including specific surface area, point of zero charge, and mineral composition, enhance the understanding of adsorption and thermodynamic pathways. Practically, the results highlight the potential of locally available bentonite as a low-cost, sustainable, and regenerable adsorbent, offering added value for industrial wastewater treatment and supporting eco-friendly remediation strategies.

Methodology

1. Preparation of the adsorbent

Bentonite was obtained in Sa Bot district, Lopburi province, Thailand. The bentonite was washed with tap water and dried in a hot-air oven. The dried adsorbent was powdered and sieved with a particle size of 150-300μm.

2. Adsorbate

The chemical structure of the malachite green dye (MG) (CI 42000, molecular weight=927.02g/mol; Merck, Germany) is displayed in (Figure 1) (Boumad et al., 2024). The stock solution was made at 500mg/L to prepare the dye solution, and it was then diluted to the necessary working solution concentrations.

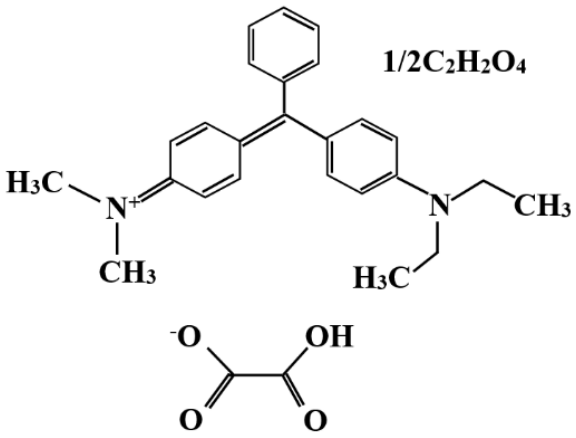

Figure 1 MG dye structure.

Source: Boumad et al., (2024)

3. Characterization of the adsorbent

The surface morphology and elemental composition were analyzed using scanning electron microscopy coupled with energy-dispersive X-ray spectroscopy (SEM-EDXS; HORIBA, Japan). Additionally, Fourier transform infrared spectroscopy (FTIR; Model Two, PerkinElmer, USA) was employed to identify the surface functional groups.

The surface area and pore structure of the bentonite were characterized via N_2 adsorption-desorption measurements at 77K using an Autosorb 1MP instrument equipped with Quantachrome NovaWin software (USA). The average pore diameter (Dp) was estimated from Equation (1).

$$Dp(nm) = \frac{4v_t \times 1000}{S_{BET}} \quad (1)$$

where V_t is the total pore volume (cm^3/g), and S_{BET} is the BET surface area (m^2/g).

4. Determination of point of zero charge (pH_{pzc})

The point of zero charge (pzc) is defined as the pH at which the net surface charge of an adsorbent equals zero. When the solution pH is below the pzc, the adsorbent surface becomes positively charged and favors anion adsorption. Conversely, at pH values above the pzc, the surface is negatively charged and favors cation adsorption. Thus, adsorption behavior strongly depends on the relationship between solution pH and the pzc value, which is determined by the intrinsic properties of the adsorbent.

To determine the point of zero charge (pH_{pzc}), a series of 100mL KCl solutions (0.01M) was prepared with initial pH values ranging from 2.0 to 12.0, adjusted using 0.10M NaOH or HCl. Subsequently, 1.0g of bentonite was added to each solution. The mixtures were stirred at room temperature for 24h, after which the final pH (pH_{final}) of each suspension was measured. The pH_{pzc} was determined by plotting the curve of each ΔpH ($pH_{final} - pH_{initial}$) against $pH_{initial}$. The pHpzc corresponds to the pH value at which the curve intersects the horizontal line where ΔpH = 0.

5. Adsorption study

The influences of adsorption, including pH (2-10), adsorbent dose (0.25-1.0g), contact time (5-240min), initial dye concentration (50-250mg/L), and temperature (20-40°C), were examined to evaluate the adsorption. Batch experiments were conducted in triplicate at 30°C using 250mL Erlenmeyer flasks containing 100mL of dye solution. The temperature-controlled orbital shaker was used for mixing the solution at a speed of 150rpm. The supernatant was collected at the designated time, and a UV-visible spectrophotometer (Analytik Jena, Specord 210 plus, Germany) at 625nm (Mahinroosta et al., 2024) was used to measure the amount of dye that was remaining in the solution. Equations (2) and (3) were used to determine the percentage of adsorption and the amount of dye adsorbed, respectively.

$$\%\ adsorption = \frac{(C_0 - C_e)\ x\ 100}{C_0} \quad (2)$$

$$q_t = \frac{(C_0 - C_t)V}{w} \quad (3)$$

where C_o (mg/L) is the initial dye concentration, Ce and C_t (mg/L) are the concentration at equilibrium and at any time, respectively; q_t (mg/g) is the amount adsorbed at any time; V(L) is the volume of the solution; and W(g) is the mass of adsorbent.

6. Adsorption isotherm

The Langmuir isotherm in a linear form is represented by Equation (4) (Ullah et al., 2021)

$$\frac{C_e}{q_e} = \frac{1}{q_{max}} c_e + \frac{1}{K_L q_m} \quad (4)$$

where C_e (mg/L) is the equilibrium concentration, q_e (mg/g) is the amount adsorbed at equilibrium, K_L is the Langmuir constant, and q_{max} (mg/g) is the maximum adsorption capacity.

The fundamental characteristics of the Langmuir isotherm can be described by a dimensionless separation factor, R_L which is defined by Equation (5)

$$R_L = \frac{1}{(1+K_L C_o)} \quad (5)$$

The Freundlich isotherm in a linear form is represented by Equation (6) (Ullah et al., 2021)

$$log\ q_e = log\ K_F + \left(\frac{1}{n}\right) log\ C_e \quad (6)$$

where K_F (L/g) is the adsorption capacity, and $\frac{1}{n}$ is the adsorption intensity.

The Redlich-Peterson isotherm in a linear form is represented by Equation (7) (Kalam et al., 2021):

$$log\ (C_e/q_e) = \beta\ log\ C_e - log\ Kr \quad (7)$$

where Kr (L/g) is the Redlich-Peterson isotherm constant and β is an exponent that ranges between 0 and 1.

7. Adsorption kinetics

Adsorption kinetic studies are essential for the treatment of aqueous effluents, as it provides critical insights into the mechanisms governing the adsorption process. In this study, the pseudo-first-order, pseudo-second-order, and intraparticle diffusion kinetic models were employed to analyze the experimental adsorption data as a function of contact time.

The pseudo-first-order kinetic model in a linear form is written as shown in Equation (8) (Ullah et al., 2021):

$$\log(q_e - q_t) = log\, q_e - \frac{k_1}{2.303} t \quad (8)$$

where k_1 (1/min) is the rate constant of pseudo-first, and q_t (mg/g) is the amount adsorbed at any time (min).

The pseudo-second order kinetic model is represented by Equation (9) (Ullah et al., 2021)

$$\frac{t}{q_t} = \frac{1}{k_2 q_e^2} + \frac{1}{q_e} t \quad (9)$$

where k_2 (g/(mg.min) is the rate constant for pseudo-second-order adsorption kinetics.

For the diffusion model of adsorption, the process is generally described in three sequential steps: (1) diffusion across the liquid film surrounding the adsorbent particles (film diffusion); (2) diffusion within the pores, known as intraparticle diffusion; and (3) adsorption–desorption interactions between the adsorbate molecules and the active sites of the adsorbent (Hasani et al., 2022). The intraparticle diffusion equation, presented in Equation (10), follows the Weber–Morris model. This model indicates that solute uptake is approximately proportional to $t^{1/2}$. The slope and intercept of the linear intraparticle diffusion plot were used to calculate the intraparticle diffusion rate constant K_{id} (mg/g.min$^{1/2}$) and the boundary layer thickness (C), respectively.

$$q_t = K_{id}\, (t)^{1/2} + C \quad (10)$$

8. Thermodynamic parameters of dye adsorption

The Gibbs free energy change (ΔG) in the adsorption process can be expressed by Equation (11)

$$\Delta G = -RT\, In\, K_c \quad (11)$$

where K_c the equilibrium constant ($K_c = (C_0\text{-}C_e)/C_e$) is employed for the thermodynamic calculations of adsorption (Keereerak & Chinpa, 2020). R is the gas constant (8.314J), and T is the absolute temperature in Kelvin (K). Also, enthalpy (ΔH) and entropy (ΔS) changes can be estimated by Equation (12)

$$log\, K_c = \frac{\Delta S}{2.303R} - \frac{\Delta H}{2.303RT} \quad (12)$$

where ΔH and ΔS can be determined respectively by the slope and intercept of the linear plot between log K_c and 1/T.

9. Statistical analysis

The adsorption capacity obtained from triplicate experiments was evaluated using the mean and the standard deviation.

Results and discussion

1. Characterization of the adsorbent

The BET method was employed to determine the specific surface area of bentonite by nitrogen adsorption at 77K. Before analysis, bentonite was degassed under vacuum at 120°C for 12h to remove moisture and volatile impurities. Although adsorption isotherms were recorded over the full relative pressure range (0-1.0), the Brunauer–Emmett–Teller (BET) equation was applied only within the interval of 0.05-0.35. This range is widely accepted as appropriate for BET analysis because it reflects the region where monolayer adsorption dominates and the BET assumptions remain valid. At higher relative pressures, multilayer adsorption and capillary condensation effects become significant, which can lead to overestimation of surface area. The monolayer adsorption capacity (Vm) was derived from the linear portion of the BET plot, and the BET constant (C) was obtained from the slope and intercept. In this study, the calculation was based on the linear region of the BET plot, corresponding to the relative pressure range of P/P_0 = 0.1418-0.2615. The specific surface area (S_{BET}) was 12.01m^2/g, with a total pore volume (V_t) of 0.0319cm^3/g. Using these values, the average pore diameter (Dp) was estimated from Equation (1), yielding 10.62nm. According to the IUPAC classification, pore diameters are categorized as micropores (d<2nm), mesopores (2-50nm), and macropores (d>50nm) (Aggarwal et al., 2025). Therefore, the bentonite used in this study was classified as mesoporous.

The relatively low BET surface area of Lopburi bentonite can be attributed to its reduced Si/Al ratio of 20.9/4.3 (Figure 3b), which contrasts with South African deposits (37.21m^2/g; Vhahangwele & Mugera, 2015) and Indian deposits (92m^2/g; Pawar et al., 2016). This compositional difference results in a denser framework and fewer micropores. Additionally, the high carbon content (32.8%, ((Figure 3b)) further contributes by coating surfaces and blocking pore accessibility, thereby limiting adsorption capacity (Huang et al., 2017). Together, these compositional factors highlight the influence of regional mineralogy and impurities on surface properties, underscoring the importance of localized characterization for optimizing bentonite utilization in textile wastewater treatment.

2. FTIR analysis

FTIR analysis (500-4,000cm^{-1}) was performed on bentonite before and after malachite green adsorption, as shown in (Figure 2). The broad band between 3,000 and 3,800cm^{-1} corresponds to the stretching vibrations of OH groups in different environments (Söğüt et al., 2021). The band at 3789cm^{-1} is assigned to Al–OH–Al groups (Borah et al., 2022), while the band at 3696cm^{-1} is attributed to the stretching vibration of OH groups coordinated to Si–OH and Al–OH (Gandhi et al., 2022). The band near 1,000cm^{-1} corresponds to the stretching vibrations of Si–O–M groups, where M can be Al or Si. Symmetric and asymmetric Si–O stretching bands were also detected with similar frequencies (Borah et al., 2022). Additionally, the bands in the 750-790cm^{-1} range are indicative of Si–O bond stretching in silicate structures (Uygun et al., 2023). The FTIR spectra of the adsorbent exhibited significant changes before and after adsorption. Before adsorption, characteristic peaks were observed at 3,789, 3,696, 1,991, 1,734, 1,366, 980 and 772cm^{-1}. The FTIR spectra of bentonite exhibited unexpected bands at 1,991, 1,734

and 1,366cm^{-1}, which are not typically associated with bentonite. In contrast, Borah et al., (2022) and Gandhi et al., (2022) did not report such bands in their spectra of purified and natural bentonite, respectively. This inconsistency with previous findings may be attributed to variations in sample origin or provenance, differences in pretreatment procedures, or the possible presence of adsorbed organic species.

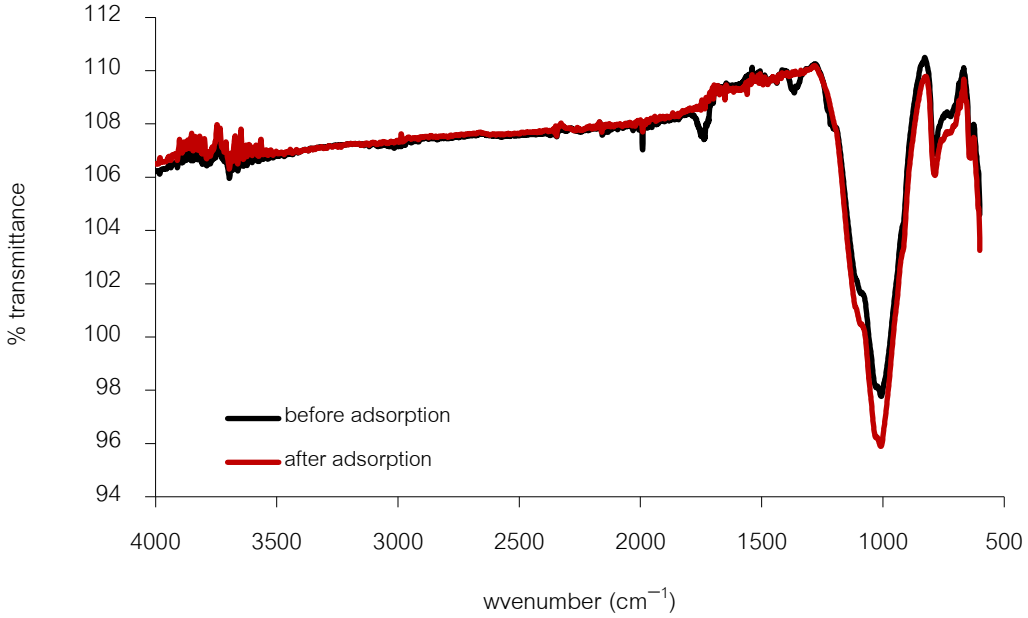

Figure 2 Fourier-transform infrared (FTIR) spectroscopy analysis before and after adsorption by bentonite.

Following the adsorption, notable shifts occurred, with peaks moving to 3,797, 3,694, 1,000, and 786cm^{-1}. These apparent peak shifts suggest the possible involvement of active aluminol (Al-OH), silanol (Si-OH), and siloxane (Si-O-Si) groups on the adsorbent surface during the uptake of malachite green. This process is likely driven by electrostatic interactions between the dye's positively charged sites and the deprotonated silanol groups (Kurniawan et al., 2012). Additionally, n-π interactions may potentially occur between the lone pair electrons (n) of the oxygen atoms in the silanol/siloxane groups and the π-electrons of the dye's aromatic rings (Zhu et al., 2018).

3. SEM-EDXS analysis

As depicted in (Figure 3a), the SEM morphology of the raw bentonite exhibits a porous, irregular, and heterogeneous surface. The presence of randomly scattered small pores suggests the availability of potential active sites that may contribute to the entrapment of MG molecules. For (Figure 3b), EDXS analysis reveals an elemental composition consisting of O (37.5%), C (32.8%), Si (20.9%), Al (4.3%), K (2.8%), and Na (1.7%) present on the surface of the adsorbent.

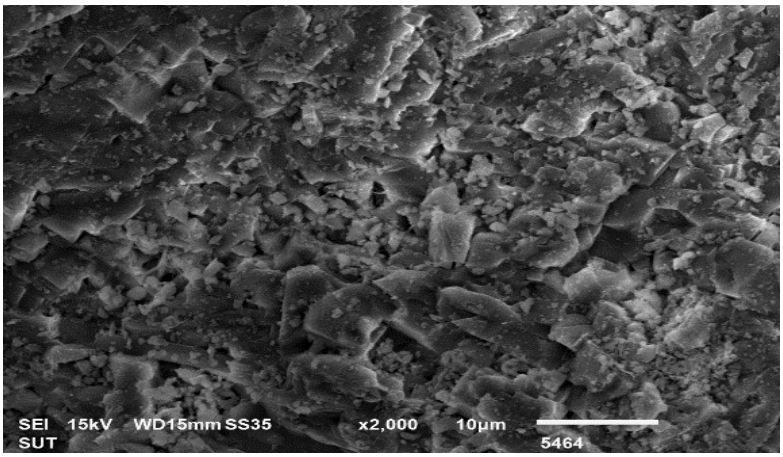

(a)

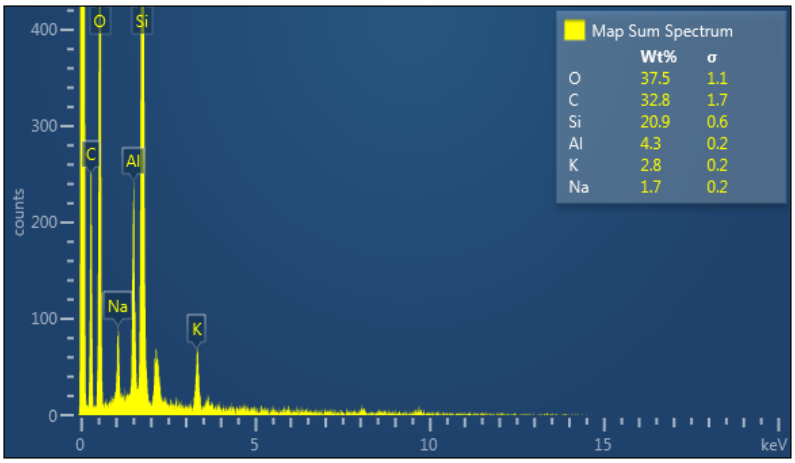

(b)

Figure 3 (a) SEM morphology and (b) EDS analysis of bentonite adsorbent.

4. Effect of pH

The pH of the solution strongly influences dye adsorption by controlling both the surface charge of the adsorbent and the ionization state of the dye. The point of zero charge (pH_{pzc}) is a critical parameter, which below this value, the adsorbent surface is positively charged, leading to electrostatic repulsion with cationic dye molecules, whereas above it, the surface becomes negatively charged, promoting electrostatic attraction and enhancing adsorption efficiency. To evaluate this effect, the initial solution pH was varied from 2.0 to 10.0 at a dye concentration of 50mg/L, a temperature of 30°C, and a bentonite dosage of 1.0g. This wide range reflects the fluctuating chemical characteristics of textile dyeing wastewater, which often exhibits alkaline conditions and heavy chemical loads depending on the batch process (Vojnović et al., 2022). Results from triplicate experiments are presented in (Figure 4). Since the pH_{pzc} of the adsorbent is 5.03 (plot not shown), the surface carries positive charges at pH values below 5.03 and negative charges above this threshold. As illustrated in (Figure 4), MG adsorption is low under acidic conditions but increases with pH, reaching a maximum at pH 9.

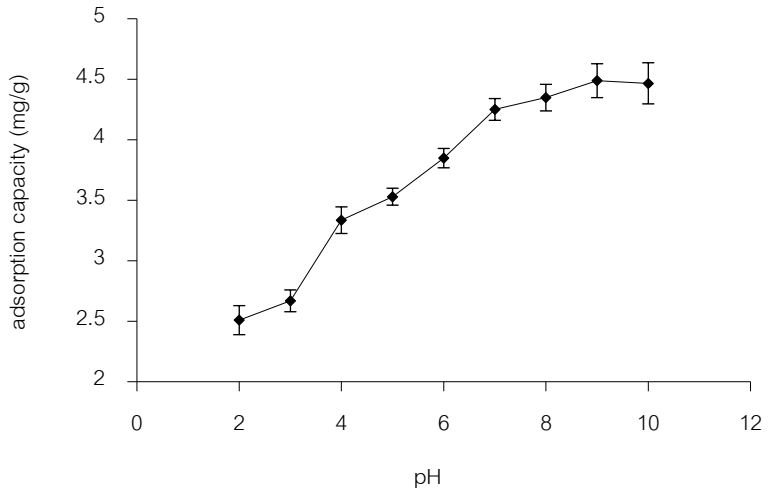

Figure 4 Effect of pH on dye adsorption (experimental conditions: 1.0g of bentonite, 180min, 30°C).

Mechanistically, at pH<5.03, protonation of bentonite surface groups imparts a net positive charge, leading to strong electrostatic repulsion with cationic MG molecules and thereby limiting adsorption efficiency (pH 2.0-4.0). Nevertheless, minor adsorption still occurs, suggesting auxiliary non-electrostatic mechanisms such as hydrogen bonding or n–π interactions (Liang et al., 2022). Conversely, at pH>5.03, deprotonation yields a negatively charged surface, intensifying electrostatic attraction toward MG and facilitating rapid dye migration to active sites. This enhancement is evident in the sharp increase in adsorption capacity from pH 4.0 to 9.0, with maximum adsorption at pH 9.0 (Ullah et al., 2021). At this optimal pH, electrostatic forces act synergistically with chemical interactions (cation exchange and hydrogen bonding), validating the comprehensive adsorption mechanism proposed in this study.

5. Effect of adsorbent dose

The adsorbent dosage is a key parameter influencing dye removal efficiency. An increasing the dosage provides a higher density of available active binding sites and a larger total surface area, thereby enhancing overall removal. Experiments were conducted with adsorbent dosages ranging from 0.25-1.0g at an initial dye concentration of 50mg/L, pH 9, temperature of 30°C, and a contact time of 240min. Results from triplicate experiments are presented in (Figure 5), showing both percent adsorption and adsorption capacity. The adsorption percentage increased (78.48, 83.65, 86.81 and 87.42%) with increasing adsorbent dosage (0.25, 0.50, 0.75, and 1.0g), owing to the greater surface area and availability of active sites (Vithalkar et al., 2022). Similar trends have been reported for COD adsorption on sugarcane bagasse–activated carbon (Sawasdee et al., 2018) and methylene blue adsorption on montmorillonite clay (Almeida et al., 2009). In contrast, the adsorption capacity decreased from 16.0 to 4.0mg/g as the dose increased. This reduction is attributed to two effects: (i) mass transfer limitation, where excessive adsorbent reduces the likelihood of MG molecules contacting active sites, thereby lowering per-unit adsorption efficiency; and (ii) pore blockage, arising from the aggregation of bentonite particles

that partially obstruct pores and limit effective surface area utilization. Although higher dosages increase overall removal rates, the sharp decline in adsorption capacity indicates underutilization of the material (Ma et al., 2026). Similar adsorption was observed for methylene blue on the milk thistle seeds (Djelloul et al., 2017).

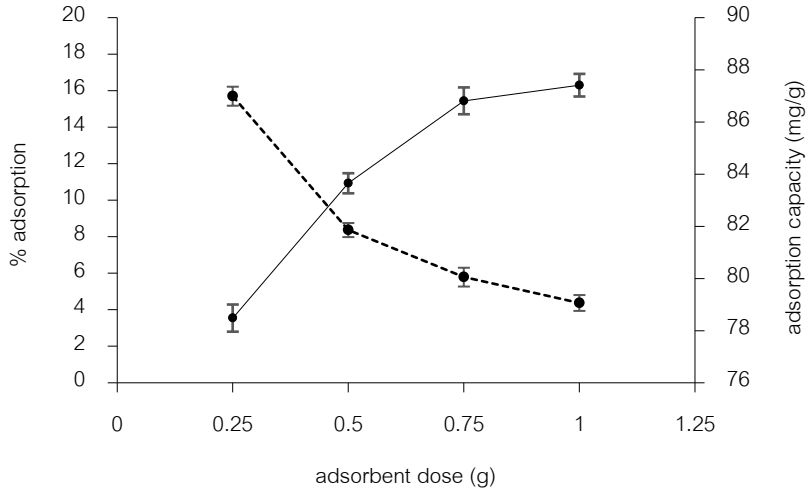

Figure 5 Effect of adsorbent dose on malachite green removal, showing the percentage adsorption (solid line) and adsorption capacity (dashed line). (experimental conditions: pH 9, 180min, 30°C).

6. Effect of contact time and initial dye concentration

Contact time governs the extent of adsorbate interaction with active sites; insufficient time leads to incomplete adsorption, while adequate time allows equilibrium and maximum uptake. Adsorbate concentration likewise controls efficiency: low concentrations favor high removal due to abundant sites, whereas higher concentrations increase competition, enhancing capacity until surface saturation is reached.

The adsorption process was investigated as a function of contact time (5-240min) at initial dye concentrations of 50 and 100mg/L, pH 9, and a temperature of 30°C, using a constant bentonite dosage of 1.0g. The results, averaged from triplicate experiments, are presented in (Figure 6). Adsorption proceeded rapidly during the first 15min, then gradually slowed, reaching equilibrium at 180 min (Ullah et al., 2021). In this phase, adsorption primarily occurs on the external surface, where accessible sites are readily available (Mansour et al., 2020). As adsorption progresses, the rate gradually decreases as readily accessible sites become occupied. Equilibrium is attained at 180min, at which point the adsorbent surface is saturated with dye molecules. This behavior reflects the transition from rapid external surface adsorption to slower intraparticle diffusion, where dye molecules migrate into the pores to access less accessible sites. Moreover, (Figure 6) shows that the adsorption capacity increased markedly with higher initial dye concentrations. At equilibrium, the capacity rose from 4.49mg/g at 50mg/L to 7.63mg/g at 100mg/L. This effect can be attributed to the stronger concentration gradient driving force observed at higher initial dye concentrations (Abewaa et al., 2023).

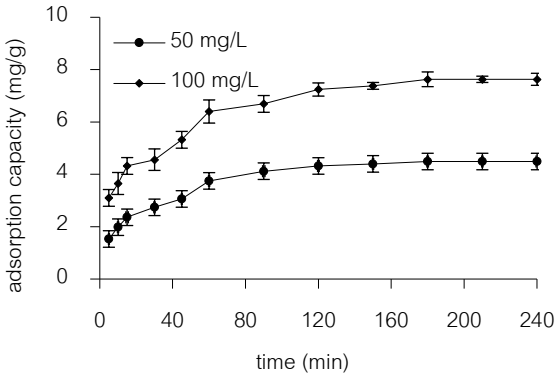

Figure 6 Effect of contact time on the adsorption capacity (mg/g). (experimental conditions: pH 9, 1.0g, 30°C).

7. Adsorption kinetics

The experimental data on the effect of contact time were analyzed using pseudo-first-order and pseudo-second-order kinetic models, as well as the intraparticle diffusion model. The linear plots are presented in (Figure 7), and the corresponding parameters are summarized in (Table 1).

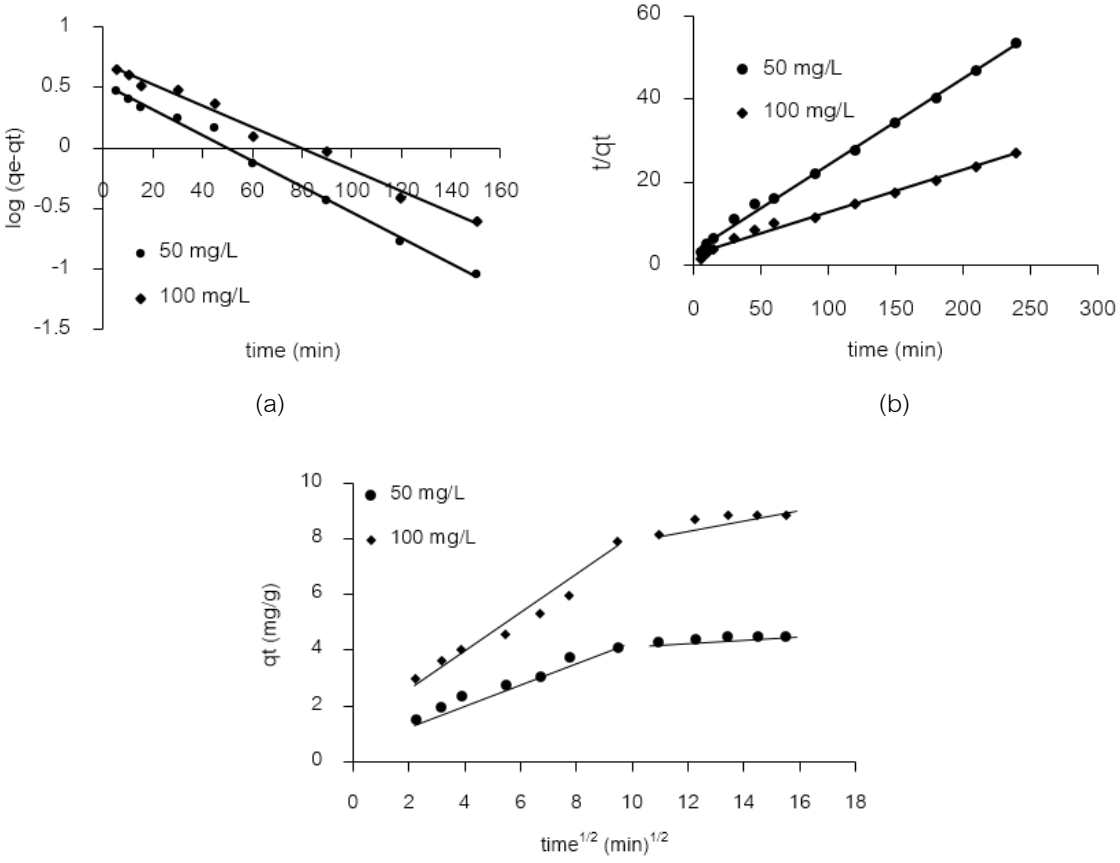

(a) (b)

(c)

Figure 7 Kinetics of dye adsorption onto bentonite: (a) pseudo-first-order model, (b) pseudo-second-order model, and (c) intraparticle diffusion model.

The linear plots of the pseudo-first-order and pseudo-second-order kinetics (Figures 7a and 7b), together with the R^2 values presented in (Table 1), demonstrate that the adsorption data are well described by the pseudo-second-order kinetic model, providing a more accurate representation of the adsorption process than the pseudo-first-order model. Furthermore, the adsorption capacities predicted by the pseudo-second-order model, 4.85 and 8.17mg/g at initial concentrations of 50 and 100mg/L, respectively, are in closer agreement with the experimentally observed values (qe,exp) of 4.49 and 8.85mg/g. This good fit indicates that the pseudo-second-order model is suitable for describing the adsorption kinetics, however, it should not be overinterpreted as direct evidence of a specific adsorption mechanism (Bullene et al., 2021). In addition, an increase in concentration led to a corresponding increase in the initial adsorption rate ($h = k_2 qe^2$). The observed h values showed an upward trend with elevated concentrations, likely due to the substantial influence of mass transfer as the driving factor (Doke & Khan, 2012).

In the intraparticle diffusion test, (Figure 7c) depicts three distinct stages of adsorption: surface adsorption, intraparticle diffusion, and equilibrium. The K_{id} values, calculated from the slopes of the second stage of the plots, were 0.092 and 0.264 at initial concentrations of 50 and 100mg/L, respectively. Since the plots do not pass through the origin, it can be inferred that intraparticle diffusion was not the sole rate-limiting step. Additional rate-limiting factors are therefore involved, with film diffusion (surface adsorption) also potentially contributing to the regulation of the overall adsorption process (Kumar, 2013). Consequently, the results suggest that the adsorption process might be simultaneously influenced by both surface adsorption and intraparticle diffusion mechanisms.

Table 1 Kinetic parameters of dye adsorption on bentonite.

kinetic models	initial dye concentration (mg/L)	
	50.000	100.000
q_e (exp) (mg/g)	4.490	8.850
pseudo-first order		
q_e (cal) (mg/g)	3.400	4.990
k_1 (1/min)	0.002	0.020
R^2	0.994	0.951
pseudo-second order		
q_e (cal) (mg/g)	4.850	8.170
k_2 (g/(mg.min))	0.012	0.005
h	0.282	0.334
R^2	0.998	0.997
intraparticle diffusion		
K_{id}	0.092	0.264
C	3.275	5.354
R^2	0.967	0.965

8. Effect of initial dye concentration on equilibrium adsorption

The adsorption was examined as a function of the initial dye concentration (50-250mg/L) under equilibrium conditions at 30°C using 1g of bentonite. The results, averaged from the triplicate experiments, are presented in (Figure 8). The equilibrium adsorption capacity increased from 4.489 to 20.387mg/g with increasing dye concentration. This behavior can be explained by the enhanced mass transfer driven by the concentration gradient, which is directly related to the initial dye concentration (Abewaa et al., 2023). As shown in (Figure 8), the plot of q_e versus C_e exhibits a curved trend and gradually approaches a plateau, indicating a favorable adsorption process that has reached saturation.

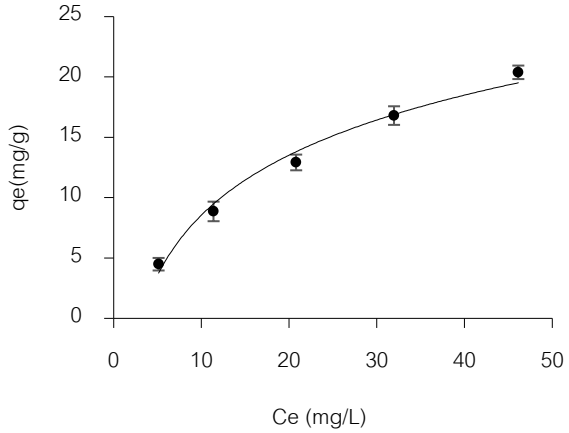

Figure 8 Effect of initial dye concentration (50-250mg/L) on equilibrium adsorption. (experimental conditions: pH 9, 1.0g, 180min, 30°C).

9. Adsorption isotherm

Adsorption isotherms describe the equilibrium relationship between the amount of adsorbate sequestered on the solid surface and its residual concentration in the liquid phase at a constant temperature. In this study, the Langmuir, Freundlich, and Redlich-Peterson isotherms were applied to analyze the adsorption data. These isotherms are fundamental in determining the maximum adsorption capacity, characterizing adsorbent properties, and elucidating the underlying adsorption mechanisms (Cui et al., 2024). To determine the adsorption isotherms, experiments were conducted with initial concentrations ranging from 50 to 250mg/L. The experimental data on the effect of initial dye concentration were analyzed using the linearized forms of the Langmuir, Freundlich, and Redlich–Peterson isotherm models, as shown in (Figure 9), and the corresponding parameters are summarized in (Table 2).

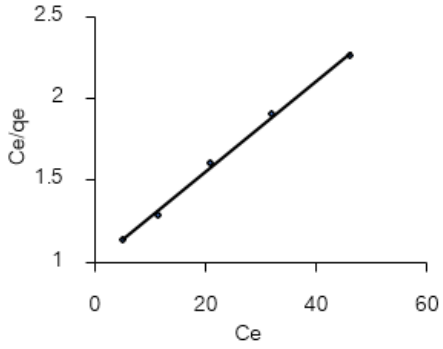

a. Langmuir isotherm

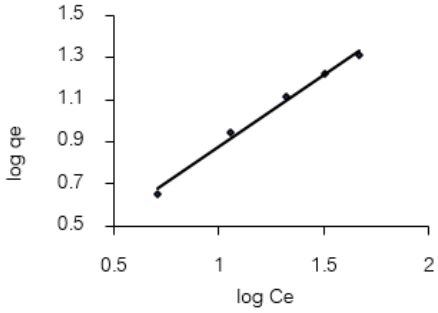

b. Freundlich isotherm

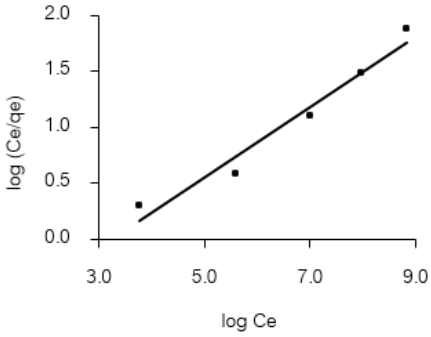

c. Redlich-Peterson isotherm

Figure 9 Isotherm plots of MG adsorption (a) Langmuir, (b) Freundlich, and (c) Redlich-Peterson isotherms.

The determination coefficients (R^2) for the Langmuir and the Freundlich models were 0.997 and 0.991, respectively. The maximum adsorption capacity (q_{max}) was 35.97mg/g at 30°C. The adsorption isotherm data were well fitted to the Langmuir isotherm, indicating that the primary chemical uptake occurs via homogeneous monolayer coverage of the adsorbate on the adsorbent surface (Waghmare et al., 2024). This favorable behavior was further confirmed by the dimensionless separation factor (R_L).

Table 2 Parameters of the isotherm models for MG dye adsorption.

isotherm model	values
Langmuir isotherm	
q_{max} (mg/g)	35.970
K_L (L/g)	0.027
R_L	0.418-0.128
R^2	0.997

Table 2 Parameters of the isotherm models for MG dye adsorption (continue).

isotherm model	values
Freundlich isotherm	
K_F (L/mg)	1.551
1/n	0.686
R^2	0.991
Redlich-Peterson isotherm	
K (L/g)	1.555
β	0.314
R^2	0.958

This parameter defines the sorption favorability as unfavorable ($R_L > 1$), favorable ($0 < R_L < 1$), linear ($R_L = 1$), or irreversible ($R_L = 0$). In this study, R_L values ranged from 0.418 to 0.128 at dye concentrations of 50-250mg/L. Since all R_L values lie within the favorable, with lower R_L values at higher concentrations implying a stronger driving force for adsorption.

The Freundlich exponent (1/n=0.686) falls within the range of 0-1, indicating favorable adsorption. Both Langmuir ($R^2 = 0.997$) and Freundlich ($R^2 = 0.991$) models provided excellent fits, suggesting that adsorption may involve monolayer coverage while surface heterogeneity also contributes. The Redlich–Peterson model yielded a lower correlation coefficient ($R^2 = 0.958$), suggesting it may not adequately capture the adsorption behavior of this system. Overall, the results suggest that monolayer adsorption is dominant, with heterogeneity of the bentonite surface playing a secondary role, and the fitted models should be regarded as indicative rather than conclusive evidence of the adsorption mechanism.

10. Comparison of bentonite and other adsorbents for MG adsorption

(Table 3) summarizes the Langmuir adsorption capacities (qmax) of malachite green (MG) using natural bentonite and other reported adsorbents. The adsorption capacity of bentonite in this study (35.97mg/g) was lower than that of several alternative materials, such as clay (180mg/g), zeolite (83.33mg/g), and Persian kaolin (52.91mg/g). However, bentonite exhibits comparable performance to coconut shell activated carbon (37.79mg/g) and wood apple shell (34.56mg/g), and superior capacity compared to diatomite (23.64mg/g). Although activated carbons and certain clays demonstrate higher adsorption capacities, their preparation costs and regeneration challenges often limit large-scale applicability. In contrast, natural bentonite offers advantages of low cost, abundance, environmental friendliness, and stable reusability over multiple cycles, making it a promising candidate for sustainable wastewater treatment. These findings suggest that while bentonite may not achieve the highest adsorption capacity, its balance of efficiency, cost-effectiveness, and regeneration potential underscores its practical relevance as an alternative adsorbent for MG removal.

Table 3 Comparison of various adsorbent materials of malachite green.

adsorbent materials	qmax	references
fig (*Ficus cartia*) leaves	51.79	Gebreslassie (2020)
persian kaolin	52.91	Tehrani-Bagha et al., (2011)
clay	180.00	Messaoudi et al., (2021)
zeolite	83.33	Abbas et al., (2023)
java apple activated carbon	64.37	Bhat et al., (2023)
coconut shells activated carbon	37.79	Piriya et al., (2023)
diatomite	23.64	Tian et al., (2016)
wood apple shell	34.56	Sartape et al., (2017)
natural bentonite	35.97	this work

11. Thermodynamics of dye adsorption

The effect of temperature (20, 30, and 40°C) on the adsorption process was investigated at an MG concentration of 50mg/L using 1g of bentonite. Experiments were performed in triplicate. Adsorption data were plotted as log Kc versus 1/T, as shown in (Figure 10). Gibbs free energy (ΔG) was calculated using Equation (11), while enthalpy (ΔH) and entropy (ΔS) changes were derived from the slope and intercept of the Van't Hoff plot (Figure 10) based on Equation (12). The resulting thermodynamic parameters are summarized in (Table 4).

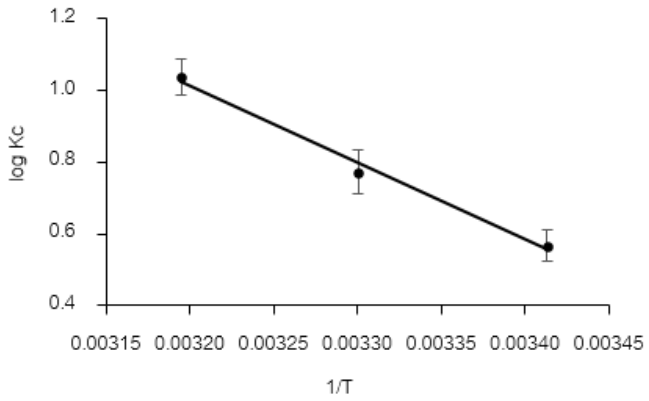

Figure 10 The plot of log K_C versus 1/T (experimental conditions: concentration 50mg/L, pH 9, 1.0g, 180min).

Table 4 Thermodynamic parameters for MG adsorption onto bentonite

temperature (°C)	ΔG (kJ/mol)	ΔH (kJ/mol)	ΔS (kJ/mol K)
20	-3.182	41.258	0.151
30	-4.327		
40	-5.823		

As shown in (Table 4), the thermodynamic parameters provide valuable insights into the adsorption behavior of MG onto bentonite. The Gibbs free energy (ΔG) values were negative at 20°C (-3.182kJ/mol), 30°C (-4.327kJ/mol), and 40°C (-5.823kJ/mol), indicating that the adsorption is favorable and spontaneous at all studied temperatures. This temperature-dependent spontaneous transition aligns with previous findings reported for malachite green adsorption onto Fig (*Ficus* cartia) leaves (Gebreslassie, 2020). Such small magnitudes are generally consistent with physisorption, where the uptake is governed by weak van der Waals forces or electrostatic interactions rather than strong chemical bonding (Mansour et al., 2020).

The magnitude of ΔH provides insight into the nature of the forces governing the adsorption process. Generally, the energy associated with chemical forces (typically > 60kJ/mol) significantly exceeds that of physical interactions, such as van der Waals forces (4-10kJ/mol), hydrophobic bonds (5kJ/mol), hydrogen bonding (2-40kJ/mol), and dipole interactions (2-29kJ/mol). In this study, the obtained ΔH value of 41.258kJ/mol confirms that the adsorption of MG onto bentonite is primarily driven by hydrogen bonding (Lafi et al., 2019). The positive entropy change (ΔS) indicates increased randomness at the solid–solution interface during MG adsorption (Cheng et al., 2017). At temperatures of 20-40°C and above, the product $T^{*}\Delta S$ exceeds ΔH; therefore, the adsorption process is governed primarily by entropy rather than enthalpy.

12. Reusability of adsorbent

Considering its cost-effectiveness, bentonite was subjected to regeneration and reusability tests for malachite green (MG) removal from aqueous solutions. The regeneration potential after each adsorption cycle was evaluated by desorbing MG with 0.1M HCl at a solid-to-liquid ratio of 1g: 100mL for 3h. Each cycle was conducted in triplicate. The regenerated bentonite was subsequently washed to neutrality and reused for MG adsorption at a concentration of 50 mg/L. Over five consecutive cycles (Figure 11), the dye removal efficiencies calculated using Equation (2) were 84.24, 79.63, 76.32, 71.12 and 68.87%, respectively. The observed decline in adsorption efficiency after repeated cycles may be attributed to incomplete restoration of the adsorbent's properties during regeneration, progressive surface saturation, or fouling effects resulting from repeated use (Hamad et al., 2024). Such deterioration is likely associated with the degradation of functional groups, which reduces the number of available active sites. Lucaci & Bulgariu (2024) further reported that desorption efficiency decreases with increasing cycles, and that protonated functional groups formed after mineral acid treatment can interact via hydrogen bonding. These bonds are not readily broken upon pH adjustment in subsequent cycles, thereby limiting regeneration efficiency and contributing to the decline in adsorption performance. Nevertheless, maintaining a removal efficiency above 68% after five cycles demonstrates that bentonite retains considerable reusability, highlighting its potential as a cost-effective and sustainable adsorbent for dye removal applications.

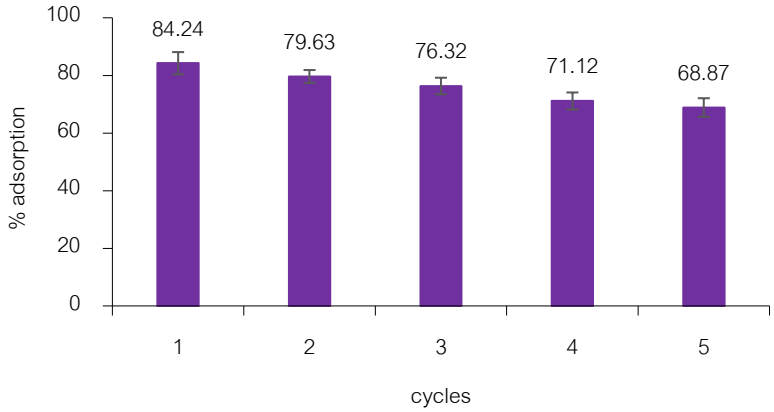

Figure 11 Reusability of bentonite for MG adsorption.

The reusability test highlights the practical potential of bentonite as an adsorbent. Although adsorption efficiency declined after repeated cycles, this reduction may be attributed to partial pore blockage or irreversible occupation of active sites, structural changes in the adsorbent, or incomplete desorption of MG molecules during regeneration. These findings emphasize the need for further studies on regeneration strategies, surface modification, and long-term stability to enhance the durability and reusability of bentonite in real wastewater treatment applications. A similar markedly reduced in adsorption capacity after multiple regeneration cycles has been documented in the literature for other biomass-derived adsorbents, such as calcined mussel shells, where the capacity significantly marked decline due to repetitive structural stress and site blockage (El Haddad, 2016).

13. Mechanism of malachite green dye adsorption

According to the results of these investigations, the adsorption mechanisms were identified and are illustrated in (Figure 12). At pH 9, the adsorption of malachite green (MG), a cationic dye, onto bentonite occurs via interactions between the dye's positively charged molecules and the adsorbents negatively charged active sites ($Al\text{-}O^{-}$ / $Si\text{-}O^{-}$). Thus, the predominant adsorption mechanism may be due to electrostatic attraction.

The adsorption mechanism involves the diffusion of adsorbate molecules into the porous network of the bentonite. Given that the BET analysis classified the prepared bentonite as a predominantly mesoporous material with an average pore diameter of 10.62nm, the intra-particle diffusion process mainly occurs within these mesoporous channels rather than micropores. The relatively wide mesopore size (10.62nm) effectively minimizes steric hindrance, allowing smooth mass transfer and accessibility for the dye/adsorbate molecules to interact with the active sites inside the pore walls

For MG adsorption, the FTIR spectra of the bentonite (Figure 2) showed Al–OH and Si–OH stretching peaks at 3,789cm^{-1} and 3,696cm^{-1}, which shifted to 3,797cm^{-1} and 3,694cm^{-1}, respectively, suggesting the possible involvement of hydrogen-bonding interactions. Similar mechanisms have been reported for crystal violet adsorption on kaolinite–bean peel composites (Mecheri et al., 2023). The observed spectral shift may contribute to the formation of Yoshida-type hydrogen bonds between bentonite hydroxyl groups and the aromatic rings of MG.

Furthermore, the peaks at 1,000cm^{-1} and 772cm^{-1}, assigned to Si–O–Si/Al and Si–O vibrations, shifted to 980cm^{-1} and 786cm^{-1}, respectively, which may contribute to n–**π** interactions between oxygen lone pairs and MG aromatic **π** electrons. The randomly distributed mesoporous structure of the adsorbent provides abundant active sites, thereby facilitating pore filling during adsorption. EDXS analysis confirmed the presence of Al, K, and Na ions on the bentonite surface, which may contribute to cation exchange with positively charged MG molecules.

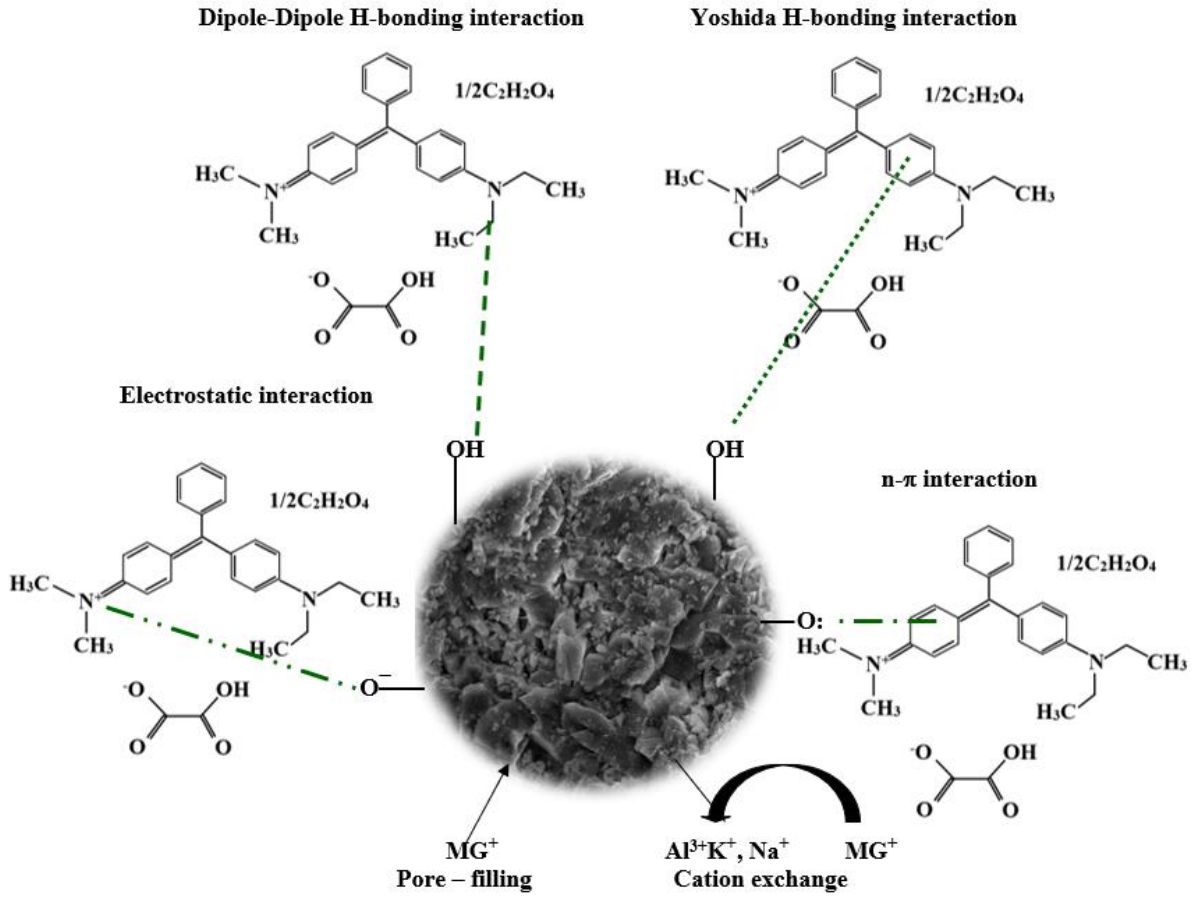

Figure 12 Mechanistic insights into malachite green adsorption onto bentonite.

Conclusion

This study demonstrated the effective utilization of bentonite as a low-cost mesoporous adsorbent for the removal of malachite green dye from aqueous solutions. The bentonite exhibited a BET surface area of 12.01m^2/g with an average pore diameter of 10.62nm, confirming its mesoporous structure and suitability for dye adsorption. Optimal removal was achieved at pH 9 with an equilibrium time of 180min. Adsorption equilibrium data were well described by the Langmuir and Freundlich models, while the Redlich–Peterson model indicated surface heterogeneity and a distribution of binding energies. Kinetic analysis revealed that the adsorption process followed a pseudo-second-order kinetic model. Thermodynamic parameters showed that adsorption is

endothermic and becomes favorable at 20-40°C. Mechanistic insights suggested that physisorption predominated, governed by electrostatic interactions, hydrogen bonding, n–π interactions, pore filling, and ion exchange. The adsorbent maintained the stable performance over five consecutive regeneration cycles, although efficiency declined slightly with repeated use. Collectively, these findings highlight the potential of natural bentonite as a cost-effective alternative to synthetic adsorbents for dye removal. Although this study was conducted on a laboratory scale, future work should explore pilot-scale and continuous-flow applications, particularly fixed-bed column studies, to assess large-scale feasibility. The adsorption system is intended for treating textile wastewater from dyeing processes, where high dye concentrations are common, underscoring its industrial relevance. A limitation of this study is the use of synthetic dye solutions, which may not fully represent real wastewater complexity. Therefore, future studies should validate the performance under realistic conditions to ensure long-term stability and practical applicability.

Acknowledgement

The authors gratefully acknowledge the institutional support provided by Thepsatri Rajabhat University, Thailand.

References

Abbas, M., & Trari, M. (2020). Removal of methylene blue in aqueous solution by economic adsorbent derived from apricot stone activated carbon. *Fibers and Polymers, 21*, 810-820. https://doi.org/10.1007/s12221-020-8630-8

Abbas, M., & Trari, M. (2023). Contribution of zeolite to remove malachite green in aqueous solution by adsorption processes: Kinetics, isotherms and thermodynamic studies. *Textile Research Journal*, *93*(15-16), 3765-3776. https://doi.org/10.1177/00405175231165336

Abewaa, M., Mengistu, A., Takele, T., Fito, J., & Nkambule, T. (2023). Adsorptive removal of malachite green dye from aqueous solution using *Rumex abyssinicus*-derived activated carbon. *Scientific Reports*, *13*(1), 14701. https://doi.org/10.1038/s41598-023-41957-x

Aggarwal, P., Umar, F., & Paul, A. (2025). Review of ordered pores in nanomaterials for energy applications ranging from energy storage to catalysis. *ACS Applied Nano Material*, *8,* 17780-17818. https://doi.org/10.1021/acsanm.5c03047

Alexander, J. A., Ahmad Zaini, M. A., Surajudeen, A., Aliyu, E. N. U., & Omeiza, A. U. (2019). Surface modification of low-cost bentonite adsorbents: A review. *Particulate Science and Technology*, *37*(5), 538-549. https://doi.org/10.1080/02726351.2018.1438548

Almeida, C. A. P., Debacher, N. A., Downs, A. I., Cottet, L., & Mello, C. A. D. (2009). Removal of methylene blue from colored effluents by adsorption on monmorillonite clay. *Journal of Colloid and Interface Science, 332*(1), 46-53. https://doi.org/10.1016/j.jcis.2008.12.012

Baidya, K. S., & Kumar, U. (2021). Adsorption of brilliant green dye from aqueous solution onto chemically modified areca nut husk. *South African Journal of Chemical Engineering*, *35*, 33-43. https://doi.org/10.1016/j.sajce.2020.11.001

Bhat, S. S., Narayana, B., & Bhat, J. I. (2023). Adsorption of malachite green dye using low-cost adsorbent derived from java apple leaves (syzyium samarangense). *Sādhanā*, *48*(3), 138. https://doi.org/10.1007/s12046-023-02214-z

Belkhodja, A., Choukchou-Braham, E., Benkhaled, A., Guendouz, S., & Attar, T. (2026). Study of the adsorption of a textile dye by alginate-bentonite beads: CCD-RSM design conception. *Journal of Macromolecular Science Part B, 65*(4), 567-589. https://doi.org/10.1080/00222348.2024.2437854

Bergaoui, M., Nakhli, A., Yeo, J. Y. J., Soetaredjo, F. E., Ismadji, S., Sunarso, J., & Khalfaoui, M. (2023). Novel insights on the adsorption ability of bentonite and its chitosan composite: Deep understanding of antibiotics removal as hazardous agents. *Journal of Molecular Liquids*, *387*, 122550. https://doi.org/10.1016/j.molliq.2023.122550

Borah, D., Nath, H., & Saikia, H. (2022). Purification of crude bentonite clay: Synthesis and characterization of Na, Mg and Cu incorporated bentonite clay. *Asian Journal of Chemistry, 34*(5), 1237-1244. https://doi.org/10.14233/ajchem.2022.23697

Boumad, S., Cano-Casanova, L., Román-Martínez, M. C., Bouchenafa-Saib, N., & Lillo-Rodenas, M. A. (2024). Removal of malachite green from water: Comparison of adsorption in a residue-derived AC versus photocatalytic oxidation with TiO_2 and study of the adsorption-photocatalysis synergy. *Environmental Research*, *250*, 118510. https://doi.org/10.1016/j.envres.2024.118510

Bullen, J. C., Saleesongsom, S., Gallagher, K., Dominik, J., & Weiss, D. J. (2021). A revised pseudo-second-order kinetic model for adsorption, sensitive to changes in adsorbate and adsorbent concentrations. *Langmuir, 37*(10), 3189-3201. https://doi.org/10.1021/acs.langmuir.1c00142

Cheng, S., Zhang, L., Xia, H., Peng, J., Shu, J., Li, C., Jiang, X., & Zhang, Q. (2017). Adsorption behavior of methylene blue on waste-derived adsorbent and exhaust gases recycling. *RSC Advances, 7*, 27331. https://doi.org/10.1039/c7ra01482a

Cui, Q., Huang, Y., Ma, X., Li, S., Bai, R., Li, H., Liu, W., & Wei, H. (2024). Research on the adsorption mechanism and performance of cotton stalk-based biochar. *Molecules*, *29*, 5841. https://doi.org/10.3390/molecules29245841

Djelloul, C., Hasseine, A., & Hamdaouic, O. (2017). Adsorption of cationic dye from aqueous solution by milk thistle seeds: Isotherm, kinetic and thermodynamic studies. *Desalination and Water Treatment, 78*, 313-320. https://doi.org/10.5004/dwt.2017.20920

Doke, K. M., & Khan, E. M. (2012). Equilibrium, kinetic, and diffusion mechanism of Cr (VI) adsorption onto activated carbon derived from wood apple shell. *Arabian Journal of Chemistry, 10*, S252-S260. https://doi.org/10.1016/j.arabjc.2012.07.031

Dutta, S., Gupta, B., Srivastava, S. K., & Gupta, A. K. (2021). Recent advances on the removal of dyes from wastewater using various adsorbents: A critical review. *Materials Advances, 2*(14), 4497-7311. https://doi.org/10.1039/d1ma00354b

El Haddad, M. (2016). Removal of basic fuchsin dye from water using mussel shell biomass waste as an adsorbent: Equilibrium, kinetics, and thermodynamics. *Journal of Taibah University for Science*, *10*(5), 664-674. https://doi.org/10.1016/j.jtusci.2015.08.007

Fernandes, J. V., Rodrigues, A. M., Menezes, R. R., & Neves, G. D. A. (2020). Adsorption of anionic dye on the acid-functionalized bentonite. *Materials*, *13*(16), 3600. https://doi.org/10.3390/ma13163600

Gandhi, D., Bandyopadhyay, R., & Soni, B. (2022). Naturally occurring bentonite clay: Structural augmentation, characterization and application as catalyst. *Material Today: Proceedings, 57*(1), 194-201. https://doi.org/10.1016/j.matpr.2022.02.346

Gebreslassie, Y. T. (2020). Equilibrium, kinetics, and thermodynamic studies of malachite green adsorption onto fig (*Ficus cartia*) leaves. *Journal of Analytical Methods in Chemistry*, *2020*(1), 7384675. https://doi.org/10.1155/2020/7384675

Hakim, Y. M., Mohadi, R., Mardiyanto., & Royani, I. (2023). Ammonium-assisted intercalation of Java bentonite as effective of cationic dye removal. *Journal of Ecological Engineering*, *24*(2), 184-195. https://doi.org/10.12911/22998993/156665

Hamad, H. N., Idrus, S., Yusuf, B., Jamali, N. S., Ahsan, A., Suhartini, S., & Wahab, A. M. A. (2024). Optimized bentonite clay adsorbents for methylene blue removal. *Processes*, *12*(4), 738. https://doi.org/10.3390/pr12040738

Hasani, N., Selimi, T., Mele, A., Thaci, V., Halili, J., Berisha, A., & Sadiku, M. (2022). Theoretical, equilibrium, kinetics and thermodynamic investigations of methylene blue adsorption onto lignite coal. *Molecules, 27*, 1856. https://doi.org/10.3390/molecules27061856

Huang, Z., Li, Y., Chen, W., Shi, J., Zhang, N., Wang, X., Li, Z., Gao, L., & Zhang, Y. (2017). Modified bentonite adsorption of organic pollutants of dye wastewater. *Materials Chemistry and Physics, 202*, 266-276. https://doi.org/10.1016/j.matchemphys.2017.09.028

Kalam, S., Abu-Khamsin, S., Kamal, M. S., & Patil, S. (2021). Surfactant adsorption isotherms: Review. *ACS Omega, 6*(48), 32342-32348. https://doi.org/10.1021/acsomega.1c04661

Kathing, C., & Saini, G. (2022). A review of various treatment methods for the removal of dyes from textile effluent. *Recent Progress in Materials*, *4*(4), 028. https://doi.org/10.21926/rpm.2204028

Keereerak, A., & Chinpa, W. (2020). A potential biosorbent from Moringa oleifera pod husk for crystal violet adsorption: Kinetics, isotherms, thermodynamic and desorption studies. *ScienceAsia, 46*(2), 186-194. https://doi.org/10.2306/scienceasia1513-1874.034

Kumar, P. S. (2013). Adsorption of Zn (II) ions from aqueous environment by surface modified strychnos potatorum seeds, a low-cost adsorbent. *Polish Journal of Chemical Technology*, *15*(3), 35-41. https://doi.org/10.2478/pjct-2013-0041

Kurniawan, A., Sutiono, H., Indraswati, N., & Ismadji, S. (2012). Removal of basic dyes in binary system by adsorption using rarasaponin–bentonite: Revisited of extended Langmuir model. *Chemical Engineering Journal, 189-190*, 264-274. https://doi.org/10.1016/j.cej.2012.02.070

Kusumlata, Ambade, B., Kumar, A., & Gautam, S. (2024). Sustainable solutions: Reviewing the future of textile dye contaminant removal with emerging biological treatments. *Limnological Review, 24*(2), 126-149. https://doi.org/10.3390/limnolrev24020007

Lafi, R., Montasser, I., & Hafiane, A. (2019). Adsorption of congo red dye from aqueous solutions by prepared activated carbon with oxygen-containing functional groups and its regeneration. *Adsorption Science & Technology*, *37*(1-2), 160-181. https://doi.org/10.1177/0263617418819227

Li, X., Wen, B., & Li, Y. (2020). Adsorption of the malachite green by magnetic clam shell powder. *Polish Journal of Environmental Studies*, *30*(1), 717-726. https://doi.org/10.15244/pjoes/123826

Liang, C., Shi, Q., Feng, J., Yao, J., Huang, H., & Xie, X. (2022). Adsorption behaviors of cationic methylene blue and anionic reactive blue 19 dyes onto nano-carbon adsorbent carbonized from small precursors. *Nanomaterials*, *12*, 1814. https://doi.org/10.3390/nano12111814

Lucaci, A. R., & Bulgariu, L. (2024). Biosorption of technologically valuable metal ions on algae wastes: Laboratory studies and applicability. *Water, 16*(4), 512. https://doi.org/10.3390/w16040512

Ma, J., Ma, Q., Wang, Q., Li, Y., Ji, W., Ma, Y., Sun, Y., & Li, Y. (2026). Synergistic enhancement of Pb^{2+} adsorption by hierarchical pore structure and ultralow Si/Al ratio in bentonite-derived sodalite. *ACS Applied Materials & Interfaces*, *18*(6), 10521-10538. https://doi.org/10.1021/acsami.5c20799

Mansour, R., Simeda, G., & Zaatout, A. (2020). Adsorption studies on brilliant green dye in aqueous solutions using activated carbon derived from guava seeds by chemical activation with phosphoric acid. *Desalination and Water Treatment, 202*, 396-409. https://doi.org/10.5004/dwt.2020.26147

Mahinroosta, M., Moattari, R. M., Allahverdi, A., & Ghadir, P. (2024). Malachite green dye removal with aluminosilicate nanopowder from aluminum dross and silicomanganese slag. *Circular Economy, 3*, 100100. https://doi.org/10.1016/j.cec.2024.100100

Mahmoud, A. S. (2022). Effect of nano bentonite on direct yellow 50 dye removal: Adsorption isotherm, kinetic analysis, and thermodynamic behavior. *Progress in Reaction Kinetics and Mechanism*, *47*, 1-23. https://doi.org/10.1177/14686783221090377

Maimulyanti, A., Prihadi, A. R., Rosita, T., & Safrudin, I. (2019). Adsorption and recovery of aroma compounds from wastewater of clove oil distillation using coffee husk biosorbent. *ScienceAsia*, *45*(5), 446. https://doi.org/10.2306/scienceasia1513-1874.2019.45.446

Mecheri, R., Zobeidi, A., Atia, S., Nacer, S. N., Salih, A. A. M., Benaissa, M., Ghernaout, D., Arni, S. A., Ghareba, S., & Elboughdiri, N. (2023). Modeling and optimizing the crystal violet dye adsorption on kaolinite mixed with cellulose waste red bean peels: Insights into the kinetic, isothermal, thermodynamic, and mechanistic study. *Materials, 16*, 4082. https://doi.org/10.3390/ma16114082

Messaoudi, M., Douma, M., Tijani, N., Dehmani, Y., & Messaoudi, L. (2021). Adsorption process of the malachite green onto clay: Kinetic and thermodynamic studies. *Desalination and Water Treatment*, *240*, 191-202. https://doi.org/10.5004/dwt.2021.27688

Momina, Mohammada, S., & Isamila, S. (2020). Study of the adsorption/desorption of MB dye solution using bentonite adsorbent coating. *Journal of Water Process Engineering, 34*, 101155. https://doi.org/10.1016/j.jwpe.2020.101155

Nirmaladevi, S., & Palanisamy, N. (2020). A comparative study of the removal of cationic and anionic dyes from aqueous solutions using biochar as an adsorbent. *Desalination and Water Treatment*, *175*, 282-292. https://doi.org/10.5004/dwt.2020.24906

Pawar, R. P., Lalhmunsiama, Bajaj, H. C., & Lee, S. M. (2016). Activated bentonite as a low-cost adsorbent for the removal of Cu(II) and Pb(II) from aqueous solutions: Batch and column studies. *Journal of Industrial and Engineering Chemistry, 34*, 213-223. https://doi.org/10.1016/j.jiec.2015.11.014

Piriya, R. S., Jayabalakrishnan, R. M., Maheswari, M., Boomiraj, K., & Oumabady, S. (2023). Comparative adsorption study of malachite green dye on acid-activated carbon. *International Journal of Environmental Analytical Chemistry*, *103*(1), 16-30. https://doi.org/10.1080/03067319.2020.1849667

Queiroga, L. N. F., Pereira, M. B. B., Silva, L. S., Filho, E. C. S., Santos, I. M. G., Fonseca, M. G., Thomas Georgelinc, T., & Jaberd, M. (2019). Microwave bentonite silylation for dye removal: Influence of the solvent. *Applied Clay Science, 168*, 478-487. https://doi.org/10.1016/j.clay.2018.11.027

Ramu, A. G., & Choi, D. (2021). Highly efficient and simultaneous catalytic reduction of multiple toxic dyes and nitrophenols waste water using highly active bimetallic PdO–NiO nanocomposite. *Scientific Reports*, *11*(1), 22699. https://doi.org/10.1038/s41598-021-01989-7

Sartape, A. S., Mandhare, A. M., Jadhav, V. V., Raut, P. D., Anuse, M. A., & Kolekar, S. S. (2017). Removal of malachite green dye from aqueous solution with adsorption technique using Limonia acidissima (wood apple) shell as low cost adsorbent. *Arabian Journal of Chemistry, 10*, S3229-S3238. https://doi.org/10.1016/j.arabjc.2013.12.019

Sawasdee, S., Chakerd, H., Pannasiri, W., & Watcharabundit, P. (2018). The COD removal in chemical laboratory wastewater by using sugarcane bagasse-activated carbon. *RMUTSB Academic Journal, 6*(1), 55-64. https://li01.tci-thaijo.org/index.php/rmutsb-sci/article/view/124253

Sehar, S., Rasool, T., Syed, H. M., Mir, M. A., Naz, I., Rehman, A., Shah, M. S., Akhter, M. S., Mahmood, Q., & Younis, A. (2022). Recent advances in biodecolorization and biodegradation of environmentally threatening textile finishing dyes. *3 Biotech*, *12*(8), 186. https://doi.org/10.1007/s13205-022-03247-7

Söğüt, E. G., Ergan, E., Kılıç, N. C., Dönmez. H., & Akbaş, E. (2021). Methylene blue adsorption from aqueous solution by functionalized perlites: An experimental and computational chemistry study. *Desalination and Water Treatment*, *217*, 391-410. https://doi.org/10.5004/dwt.2021.26752

Taibi, Z., Bentaleb, K., Bouberka, Z., Pierlot, C., Vandewalle, M., Volkringer, C., Supiot, P., & Maschke, U. (2023). Adsorption of orange G dye on hydrophobic activated bentonite from aqueous solution. *Crystals*, *13*(2), 211. https://doi.org/10.3390/cryst13020211

Tian, L., Zhang, J., Shi, H., Li, N., & Ping, Q. (2016). Adsorption of malachite green by diatomite: Equilibrium isotherms and kinetic studies. *Journal of Dispersion Science and Technology, 37*, 1059-1066. https://doi.org/10.1080/01932691.2015.1080610

Tehrani-Bagha, A. R., Nikkar, H., Mahmoodi, N. M., Markazi, M., & Menger, F. M. (2011). The sorption of cationic dyes onto kaolin: Kinetic, isotherm and thermodynamic studies. *Desalination*, *266*(1-3), 274-280. https://doi.org/10.1016/j.desal.2010.08.036

Ukkund, S. J., Puthiyillam, P., Alshehri, H. M., Goodarzi, M., Taqui, S. N., Anqi, A. E., Safaei, M. R., Ali, M. A., Syed, U. T., Mir, R. A., Elfasakhany, A., Eed, E. M., Siddiqui, M. I. H., Mokashi, I., & Soudagar, M. E. M. (2021). Adsorption method for the remediation of brilliant green dye using halloysite nanotube: Isotherm, kinetic and modeling studies. *Applied Sciences*, *11*, 8088. https://doi.org/10.3390/app11178088

Ullah, S., Ur Rahman, A., Ullah, F., Rashid, A., Arshad, T., Viglašová, E., Galamboš, M., Mahmoodi, M., & Ullah, H. (2021). Adsorption of malachite green dye onto mesoporous natural inorganic clays: Their equilibrium isotherm and kinetics studies. *Water*, *13*(7), 965. https://doi.org/10.3390/w13070965

Uygun, O., Güven, R., & Çakal, G. Ö. (2023). Adsorptive removal of stable and radioactive Pb (II) isotopes from aqueous solution using bentonite, zeolite and perlite: Characterization, isotherm and thermodynamic studies. *Clay Minerals*, *58*(2), 195-209. https://doi.org/10.1180/clm.2023.18

Vhahangwele, M., & Mugera, G. (2015). The potential of ball-milled South African bentonite clay for attenuation of heavy metals from acidic wastewater: Simultaneous sorption of Co^{2+}, Cu^{2+}, Ni^{2+}, Pb^{2+} and Zn^{2+} ions. *Journal of Environmental Chemical Engineering*, *3,* 2416-2425. https://doi.org/10.1016/j.jece.2015.08.016

Vithalkar, S., Jugade, R. M., & Saravanan, D. (2022). Adsorption of brilliant green dye by used-tea-powder: Equilibrium, kinetics and thermodynamics studies. *Water Infrastructure, Ecosystems and Society*, *71*(10), 1148-1158. https://doi.org/10.2166/aqua.2022.076

Vojnović, B., Cetina, M., Franjković, P., & Sutlović, A. (2022). Influence of initial ph value on the adsorption of reactive black 5 dye on powdered activated carbon: Kinetics, mechanisms, and thermodynamics. *Molecules*, *27*(4), 1349. https://doi.org/10.3390/molecules27041349

Waghmare, C., Ghodmare, S., Ansari, K., Alfaisal, F. M., Alam, S., Khan, M. A., & Ezaier, Y. (2024). Adsorption of methylene blue dye onto phosphoric acid-treated pomegranate peel adsorbent: Kinetic

and thermodynamic studies. *Desalination and Water Treatment, 318*, 100406. https://doi.org/10.1016/j.dwt.2024.100406

Zhu, Y., Yi, B., Yuan, Q., Wu, Y., Wang, M., & Yan, S. (2018). Removal of methylene blue from aqueous solution by cattle manure-derived low temperature biochar. *RSC Advances*, *8*(36), 19917-19929. https://doi.org/10.1039/c8ra03018a